Assembly and Molecular Architecture of the p85α homodimer

Jaclyn LoPiccolo[1,§], Seung Joong Kim[4,§], Yi Shi[5], Bin Wu[3], Haiyan Wu[1], Brian T. Chait[5], Robert Singer[3], Andrej Sali[4], Michael Brenowitz[2], Anne R. Bresnick[2], and Jonathan M. Backer[1,2]

[1]Department of Molecular Pharmacology, [2]Department of Biochemistry, [3]Department of Anatomy and Structural Biology, Albert Einstein College of Medicine, Bronx, NY 10461, USA

[4]Department of Bioengineering and Therapeutic Sciences and Department of Pharmaceutical Chemistry, California Institute for Quantitative Biosciences, Byers Hall, 1700 4th Street, Suite 503B, University of California, San Francisco, San Francisco, CA 94158, USA

[5]Laboratory of Mass Spectrometry and Gaseous Ion Chemistry, The Rockefeller University, New York, NY 10065, USA

Running title: *Molecular Architecture of the p85α homodimer*

[§]These authors contributed equally to this work.

To whom correspondence should be addressed: Jonathan M. Backer, MD, Department of Molecular Pharmacology, Albert Einstein College of Medicine, 1300 Morris Park Ave., Bronx, NY 10461, USA, Tel: 718-430-2153; E-mail: jonathan.backer@einstein.yu.edu; Anne R. Bresnick, PhD., Department of Biochemistry, Albert Einstein College of Medicine, 1300 Morris Park Ave., Bronx, NY 10461, USA, Tel: 718 430-2741; Email: anne.bresnick@einstein.yu.edu; Michael Brenowitz, Ph.D., Department of Biology, Albert Einstein College of Medicine, 1300 Morris Park Ave., Bronx, NY, USA, 10461, Tel: 718 430-3179, Email: michael.brenowitz@einstein.yu.edu.

Keywords: phosphatidylinositide 3-kinase (PI 3-kinase), phosphatidylinositol signaling, analytical ultracentrifugation, small-angle X-ray scattering (SAXS), molecular modeling, structural model

SUPPLEMENTAL METHODS

Small angle X-ray scattering (SAXS)—SAXS measurements of full-length and truncated p85α (Figures 3B and 4B; Supplemental Table S1, S2, and S3) were carried out at Beamline 4-2 of the Stanford Synchrotron Radiation Lightsource (SSRL) in the SLAC National Accelerator Laboratory. At SSRL, the beam energy and current were 11 keV and 500 mA, respectively. A silver behenate sample was used to calibrate the q-range and detector distance. Data collection was controlled with Blu-Ice (1). We used an automatic sample delivery system equipped with a 1.5 mm-diameter thin-wall quartz capillary within which a sample aliquot was oscillated in the X-ray beam to minimize radiation damage (2). The sample was placed at 1.7 meter from a MX225-HE (Rayonix, USA) CCD detector with a binned pixel size of 293 μm by 293 μm.

Up to 24 one-second exposures were made for each of the protein samples and buffers maintained at 10-25ºC. Each of the resulting diffraction images was scaled using the transmitted beam intensity, azimuthally integrated by SASTool (3), and averaged to obtain fully processed data in the form of intensity versus q [$q=4\pi\sin(\theta)/\lambda$, θ=one-half of the scattering angle; λ=X-ray wavelength].

Integrative multi-state modeling
(Stage 2) Representation of subunits and translation of the data into spatial restraints

Building an initial model of the p85α and p85α$^{1-333}$ dimers—The size and shape information contained in SAXS profiles can be used to improve the accuracy of atomic comparative models. An initial atomic model of the p85α dimer was built based on template structures (Stage 1) and SAXS profiles (Supplemental Table S1) as follows. First, we built 100 atomic comparative models for p85α "*monomer*" in complex with the SH3-binding PR1-like peptide (RPLPPRPGA), using MODELLER 9.14 (4) based on the crystal structures and the closest template structures (Stage 1 and Supplemental Table S6). The theoretical SAXS profile and the χ value of the fit to the experimental "*monomer*" SAXS profile were calculated for each of the 100 comparative models, using FoXS (5,6). Then, these 100 models were ranked by the χ value of the fit. Second, the best-scoring "*monomer*" model (with a lowest χ value) was used as a template for building an initial model of the p85α dimer. We added another copy of the p85α "*monomer"* at a random starting position for each sampling run, which resulted in an initial model of the p85α dimer. The SH3-binding PR1-like peptides were removed in the dimer model of p85α, to reflect the composition of the SAXS sample.

Next, a "*monomer*" model of p85α$^{1-333}$ was obtained by removing residues of 334-724 in the best-scoring p85α "*monomer*" model. Similarly, we added another copy of the p85α$^{1-333}$ "*monomer*" at a random starting position for each sampling run, which resulted in an initial model of the p85α$^{1-333}$ dimer. The SH3-binding PR1-like peptides were removed in the dimer model p85α$^{1-333}$, to reflect the composition of the SAXS sample.

Coarse-grained representation and spatial restraints—Domains were coarse-grained using beads representing individual residues; the coordinates of a bead were those of the corresponding C_α atoms. In a rigid body, the beads have their relative distances constrained during conformational sampling in Stage 3, whereas in a flexible string the beads are restrained by the sequence connectivity, as described later in this section. Different subsets of the spatial restraints and constraints (*i.e.*, restraint subsets) were used for different sampling runs, to improve sampling efficiency (Supplemental tables S4 and S5).

The cross-link restraints were applied to the corresponding bead pairs, taking into account the ambiguity resulting from two identical p85α subunits in a dimer; an ambiguous cross-link restraint considers all possible pair-wise assignments. For example, a restraint between residues 438 and 519 is evaluated (7) on distances:
"438@p85α.*1* − 519@p85α.*1*",
"438@p85α.*1* − 519@p85α.*2*",
"438@p85α.*2* − 519@p85α.*1*", and
"438@p85α.*2* − 519@p85α.*2*",
followed by scoring only the least violated distance.

The excluded volume restraints were applied to each bead, using the statistical relationship between the volume and the residue that it covered (8-10).

We applied the sequence connectivity restraint, using a harmonic upper-bound function of the distance between consecutive beads in a subunit, with a threshold distance equal to four times the sum of the radii of the two connected beads. The bead radius was calculated from the excluded volume of the corresponding bead, assuming standard protein density (8-11).

231 DSS chemical cross-links for the p85α dimer and 25 DST chemical cross-links for the p85α$^{1-333}$ dimer were used to restrain the distances spanned by the cross-linked residues, corresponding to the restraint subset (Tables S4 and S5). Notably, we applied 5 upper-harmonic distance restraints on residues 14-92, 51-92, 54-92, 70-92, and 73-92 (up to 13.5 Å) to retain the intermolecular interaction sites between SH3 and PR1 domains (PDB: 1PRL) (12), each one residing in a different subunit of the dimer. First, both single (restraint subsets 1 and 2 in Table S4) and double (restraint sub-

sets 3 and 4 in Table S4) intermolecular SH3-PR1 interactions were evaluated through the multi-state search for the p85α$^{1-333}$ dimer, leading to a conclusion that the double intermolecular SH3-PR1 interactions are dominant in the p85α dimer. Thus, we confined double intermolecular SH3-PR1 interactions in all restraint subsets of the p85α dimer (Table S5).

4 homo-dimer cross-links between residues 438-438, 480-480, 530-530, and 567-567 were transformed to upper-harmonic distance restraints (up to 20 Å), enforcing the parallel intermolecular orientation of two iSH2 domains (restraint subsets 1, 2, 3, 10, and 11 in Table S5). In contrast, 4 chemical cross-links of 438-519, 438-530, 447-519, and 447-530 were transformed to upper-harmonic distance restraints (up to 20 Å), enforcing the anti-parallel intermolecular orientation of two iSH2 domains (restraint subsets 4, 5, 6, 12, and 13 in Table S5). In addition, a homo-dimer cross-link of 633-633 was transformed to upper-harmonic distance restraints (up to 20 Å), enforcing the intermolecular interaction of two cSH2 domains (all restraint subsets in Table S5).

Lastly, a most populated state of the p85α$^{1-333}$ dimer (40.3% population) was further constrained during conformational sampling of the p85α dimer, in selected restraint subsets 10 to 15 but not restraint subsets 1 to 9 (Table S5).

(Stage 3) Conformational sampling to produce a most parsimonious multi-state model consistent with all available data and information

For each of the restraint subsets, 2 to 3 independent sampling calculations were performed, each one starting with a random initial configuration (Supplemental Tables S4 and S5). 4 to 16 replicas were used with temperatures ranging between 1.0 and 2.5. A model was saved every 10 Gibbs sampling steps, each consisting of a cycle of Monte Carlo steps that moved every rigid body and flexible bead once (10).

The *multi-state SAXS score* (13) is the χ value for the comparison of the *multi-state SAXS profile* to the experimental profile; the *multi-state SAXS profile* is a weighted average of the theoretical SAXS profiles for the selected subset of states, each one calculated using FoXS (5,6). The side chains of whole residues in each state were reconstructed using PULCHRA 3.06 (14) for higher accuracy in the theoretical SAXS profiles.

The *multi-state cross-link score* is a negative value of the proportion of chemical cross-links satisfied in the selected subset of states; a cross-link restraint was considered to be satisfied by the subset if the minimum $C_\alpha - C_\alpha$ distance of the corresponding residue pairs was smaller than a distance threshold of 35 Å, considering restraint ambiguity (above).

SUPPLEMENTAL FIGURE LEGENDS

FIGURE S1. Sedimentation equilibrium analysis of p85α using SH3-binding proline rich peptide.
A) Weight average molecular weights (in kDa) obtained from sedimentation equilibrium of p85α alone or in the presence of either 1 mM or 10 mM SH3-binding peptide in 20 mM NaCl (left) or 500 mM NaCl (right) at 10 °C.

B) Weight average molecular weights (in kDa) obtained from sedimentation equilibrium of p85α with 0.25, 0.5, or 1 mM SH3-binding peptide in 500 mM NaCl at 25 °C.

FIGURE S2. Sedimentation equilibrium analysis of p85α at 10 °C.
The graphs show the distribution of p85α protein concentration during sedimentation equilibrium analysis at 10 °C obtained by measuring the absorption at 280 nm versus the radial distance from the center of the rotor. Three concentrations of full-length p85α were analyzed (1.2, 3.6, and 9.6 μM). The equilibrium protein concentration distributions measured at each of the two rotor speeds are shown (upper curve: 8,000 rpm; lower curve: 16,000 rpm) with the best fit to a monomer-dimer association model shown as the solid grey line. The residuals for the fit are shown by the symbols along the dotted line at 0.0.

FIGURE S3. Sedimentation equilibrium analysis of the p85α BCR domain.
Weight average molecular weights (kDa) obtained from sedimentation equilibrium of native and cysteine-free $p85\alpha^{78-322}$ at 4 °C, 10 °C, and 37 °C. Dashed line indicates calculated MW of monomer (28.8 kDa).

FIGURE S4. Integrative multi-state modeling of the p85α dimers.

The approach proceeds through four stages: (1) gathering of data, (2) representation of subunits and translation of the data into spatial restraints, (3) conformational sampling to produce a most parsimonious multi-state model consistent with all available data and information, and (4) analysis and assessment of the multi-state model. Our protocol was scripted using the Python Modeling Interface (PMI), version 2f82087, a library for modeling macromolecular complexes based on our open-source Integrative Modeling Platform package release 2.5 (http://salilab.org/imp) (8,15-20). Files for the input data, scripts, and output model structures in multiple states are available at http://salilab.org/p85.

FIGURE S5. **Consistency between the chemical cross-links and the multi-state model of the p85α dimers**
(Left) The green dots represent cross-linked residue pairs satisfied by the corresponding multi-state model within the distance threshold of 35 Å. The red dots represent cross-linked residue pairs that violated the distance threshold of 35 Å. The blue dots represent 5 homo-dimer cross-linked residue pairs identified between two subunits in the dimer. As a result, the multi-state model of the $p85\alpha^{1-333}$ dimer satisfied all 25 DST chemical cross-links (Top), and the multi-state model of the p85α dimer satisfied 244 (95%) of the combined 256 (25 DST and 231 DSS) cross-links (Bottom).
(Right) Histograms of Euclidean C_α pair distances are shown for the chemical cross-links assessed against the multi-state models.

FIGURE S6. **Consistency between the 25 DST chemical cross-links and the individual states of the $p85\alpha^{1-333}$ dimer**

(1st and 2nd columns) Each of the 5 states in the multi-state model, along with population weights and domain labels, is shown. 25 DST chemical cross-links are visualized as blue (satisfied) and red (violated) lines connecting the corresponding residue pair in each state, using Xlink Analyzer (21). Colors were adjusted to distinguish individual domains in the dimer.
(3rd column) The green dots represent cross-linked residue pairs satisfied by the corresponding state of the $p85\alpha^{1-333}$ dimer within the distance threshold of 35 Å. The red dots represent cross-linked residue pairs that violated the distance threshold of 35 Å. The blue dots represent 5 homo-dimer cross-linked residue pairs identified between two subunits in the dimer.
(4th column) Histograms of Euclidean C_α pair distances are shown for the chemical cross-links assessed against the corresponding state.
(5th column) We assessed the 25 DST chemical cross-links against the individual $p85\alpha^{1-333}$ subunits in each of the 5 states. The diagonal insets show the cross-link evaluation maps within the same $p85\alpha^{1-333}$ subunit itself (p85α.*1* − p85α.*1* or p85α.*2* − p85α.*2*), thus exploring the intra-molecular cross-links in the corresponding state. The off-diagonal insets show the cross-link evaluation maps between the opposing $p85\alpha^{1-333}$ subunits (p85α.*1* − p85α.*2* or p85α.*2* − p85α.*1*), thus exploring the inter-molecular cross-links in the corresponding state.

FIGURE S7. **Consistency between the combined 256 (25 DST and 231 DSS) chemical cross-links and the individual states of the p85α dimer**
(1st and 2nd columns) Each of the 5 states in the multi-state model, along with population weights and domain labels. Combined 256 chemical cross-links are visualized as blue (satisfied) and red (violated) lines connecting the corresponding residue pair in each state, using Xlink Analyzer (21). Colors were adjusted to distinguish individual domains in the dimer.
(3rd column) The green dots represent cross-linked residue pairs satisfied by the corresponding state of the p85α dimer within the distance threshold of 35 Å. The red dots represent cross-linked residue pairs that violated the distance threshold of 35 Å. The blue dots represent 5 homo-dimer cross-linked residue pairs identified between two subunits in the dimer.
(4th column) Histograms of Euclidean C_α pair distances are shown for the chemical cross-links assessed against the corresponding state.
(5th column) We assessed the combined 256 chemical cross-links against the individual p85α subunits in each of the 5 states. The diagonal insets show the cross-link evaluation maps within the same p85α subunit itself (p85α.*1* − p85α.*1* or p85α.*2* − p85α.*2*), thus exploring the intra-molecular cross-links in the corresponding state. The off-diagonal insets show the cross-link evaluation maps between the opposing p85α subunits (p85α.*1* − p85α.*2* or p85α.*2* − p85α.*1*), thus exploring the inter-molecular cross-links in the corresponding state.

SUPPLEMENTAL TABLE LEGENDS

For Tables S1-S3 - SAXS parameters obtained under the conditions favoring the dimer state were highlighted in brown; those obtained under monomer conditions in blue.

*Molecular weights (*M.W.*) were estimated using SAXS MOW (22) with a threshold of Q_{max} = 0.2~0.3 (Å^{-1}), depending on the data. †SAXS data has higher noise at low concentrations (~0.5 mg/mL) than at high concentrations.

TABLE S1. Summary of SAXS analysis for full-length p85α

Tables (A) - (C) summarize SAXS parameters of molecular weight (*M.W.*), radius of gyration (R_g), and maximum particle size (D_{max}) calculated from SAXS profiles of full-length p85α, under various conditions; (A) in a low salt (20 mM NaCl) buffer at 10 and 25 °C; (B) in a high salt (500 mM) buffer at 25 °C; (C) in a high salt (500 mM NaCl) buffer at temperatures of 10°C and 25°C, with the SH3-binding PR1-like peptide.

At low salt, we observed predominantly p85α dimer at protein concentrations of 12 μM (1.0 mg/mL) at 10°C and 18 μM (1.5 mg/mL) at 25°C. Saturating concentrations of the SH3-binding PR1-like peptide drove the equilibrium completely to monomer as measured by AUC.

TABLE S2. Summary of SAXS analysis for p85α$^{1-333}$ and p85α$^{78-322}$

Tables (A) - (B) summarize SAXS parameters of molecular weight (*M.W.*), radius of gyration (R_g), and maximum particle size (D_{max}) calculated from SAXS profiles of p85α$^{1-333}$, under various conditions; (A) in a low salt (20 mM) buffer at 10 °C, with or without the SH3-binding PR1-like peptide; (B) in a high salt (500 mM) buffer at 25 °C, with or without the SH3-binding PR1-like peptide. p85α$^{1-333}$ dimerizes at sample concentrations higher than 3.5 mg/mL (92.8 μM), while it remains in a monomer state with the SH3-binding PR1-like peptide.

Tables (C) - (D) summarize SAXS parameters of molecular weight (*M.W.*), radius of gyration (R_g), and maximum particle size (D_{max}) calculated from SAXS profiles of p85α$^{78-322}$, under various conditions; (C) in a low salt (20 mM) buffer at 10 °C; (D) in a high salt (500 mM) buffer at 10 °C. p85α$^{78-322}$ remains in a monomer state under any condition, confirming that the intermolecular SH3-PR1 interaction contributes to dimerization.

TABLE S3. Summary of SAXS analysis for p85α$^{1-432}$ and p85α$^{1-600}$

Tables (A) - (B) summarize SAXS parameters of molecular weight (*M.W.*), radius of gyration (R_g), and maximum particle size (D_{max}) calculated from SAXS profiles of p85α$^{1-432}$, under various conditions; (A) in a low salt (20 mM) buffer at 10 °C, with or without the SH3-binding PR1-like peptide; (B) in a high salt (500 mM) buffer at 10 °C, with or without the SH3-binding PR1-like peptide. p85α$^{1-432}$ dimerizes at high sample concentrations of ~5.0 mg/mL (102.5 μM), while it remains in a monomer state with the SH3-binding PR1-like peptide.

Tables (C) - (D) summarize SAXS parameters of molecular weight (*M.W.*), radius of gyration (R_g), and maximum particle size (D_{max}) calculated from SAXS profiles of p85α$^{1-600}$, under various conditions; (C) in a low salt (20 mM) buffer at 10 °C, with or without the SH3-binding PR1-like peptide; (D) in a high salt (500 mM) buffer at 10 °C, with or without the SH3-binding PR1-like peptide. p85α$^{1-600}$ dimerizes at sample concentrations higher than 2.0 mg/mL (28.6 μM), while it remains in a monomer state with the SH3-binding PR1-like peptide.

Tables (A) - (D) show that the salt dependence of dimerization resides within the cSH2 domain (residues 617 to 724). The analysis also suggests that the iSH2 domain (residues 430 to 600) makes a small (two-fold) contribution to p85α dimerization.

TABLES S4 AND S5. Restraint subsets for the p85α$^{1-333}$ dimer (Table S4) and the full-length p85α dimer (Table S5), respectively

Different subsets of the spatial restraints and constraints (*i.e.*, restraint subsets) were used for different sampling runs, to improve conformational sampling efficiency. The conformational sampling produced ~80,000 (from 8 independent runs of the p85α$^{1-333}$ dimer, Table S4) and ~200,000 models (from 45 independent runs of the p85α dimer, Table S5), respectively.

We applied 5 upper-harmonic distance restraints on residues 14-92, 51-92, 54-92, 70-92, and 73-92 (up to 13.5 Å) to retain the intermolecular interaction sites between SH3 and PR1 domains (PDB: 1PRL) (12), each one residing in a different subunit of the dimer. First, both single (restraint subsets 1 and 2 in Table S4) and double (restraint subsets 3 and 4 in Table S4) intermolecular SH3-PR1 interactions were evaluated through the multi-state search for the p85α$^{1-333}$ dimer, leading to a conclusion that the double intermolecular SH3-PR1 interactions are dominant in the p85α dimer. Thus, we confined double intermolecular SH3-PR1 interactions in all restraint subsets of the p85α dimer (Table S5).

4 homo-dimer cross-links of 438-438, 480-480, 530-530, and 567-567 were transformed to upper-harmonic distance restraints (up to 20 Å), enforcing the parallel intermolecular orientation of two iSH2 domains (restraint subsets 1, 2, 3, 10, and 11 in Table S5). In contrast, 4 chemical cross-links of 438-519, 438-530, 447-519, and 447-530 were transformed to upper-harmonic distance restraints (up to 20 Å), enforcing the anti-parallel intermolecular orientation of two iSH2 domains (restraint subsets 4, 5, 6, 12, and 13 in Table S5). In addition, a homo-dimer cross-link of 633-633 was transformed to upper-harmonic distance restraints (up to 20 Å), enforcing the intermolecular interaction of two cSH2 domains (all restraint subsets in Table S5).

Lastly, a most populated state of the p85α$^{1-333}$ dimer (40.3% population) was further constrained during conformational sampling of the p85α dimer, in selected restraint subsets 10 to 15, but not restraint subsets 1 to 9 (Table S5).

TABLE S6. Representation of the p85α domains for integrative multi-state modeling

The domains of the p85α were coarse-grained using beads representing individual residues and arranged into either a rigid body (column 4) or a flexible string (column 5) based on the available crystallographic structures or comparative models. The PR1 and PR2 motifs, and 2 linkers between rigid bodies are highlighted in red in columns 1, 3, and 5. The atomic structures of the p85α domains have been previously determined through X-ray crystallography and NMR (column 3). Initial comparative models were built using MODELLER 9.14 (4) as described above, based on these atomic template structures.

TABLE S7. Consistency between the 25 DST chemical cross-links and the multi-state model of the p85α$^{1-333}$ dimer

Euclidean C_α pair distances of the 25 DST chemical cross-links were calculated for the multi-state model of the p85α$^{1-333}$ dimer. Only a shortest pair distance among the 5 states was used for assessment of an observed chemical cross-link in the multi-state model (See also cross-link evaluation maps and histograms in Supplemental Figures S5 and S6). The blue cells in the table represent chemical cross-links that were satisfied by the multi-state model or the corresponding individual state, within the distance threshold of 35 Å. In contrast, the red cells represent chemical cross-links that violated the distance threshold of 35 Å.

TABLE S8. Consistency between the combined 256 (25 DST and 231 DSS) chemical cross-links and the multi-state model of the full-length p85α dimer

Euclidean C_α pair distances of the 25 DST and 231 DSS chemical cross-links (combined in the table) were calculated for the multi-state model of the full-length p85α dimer. Only a shortest pair distance among the 5 states was used for assessment of an observed chemical cross-link in the multi-state model (See also cross-link evaluation maps and histograms in Supplemental Figures S5 and S7). The blue cells in the table represent chemical cross-links that were satisfied by the multi-state model or the corresponding individual state, within the distance threshold of 35

Å. In contrast, the red cells represent chemical cross-links that violated the distance threshold of 35 Å.

SUPPLEMENTAL REFERENCES

1. McPhillips, T. M., McPhillips, S. E., Chiu, H. J., Cohen, A. E., Deacon, A. M., Ellis, P. J., Garman, E., Gonzalez, A., Sauter, N. K., Phizackerley, R. P., Soltis, S. M., and Kuhn, P. (2002) Blu-Ice and the Distributed Control System: software for data acquisition and instrument control at macromolecular crystallography beamlines. *Journal of synchrotron radiation* **9**, 401-406
2. Martel, A., Liu, P., Weiss, T. M., Niebuhr, M., and Tsuruta, H. (2012) An integrated high-throughput data acquisition system for biological solution X-ray scattering studies. *Journal of synchrotron radiation* **19**, 431-434
3. SASTool 2013.
4. Sali, A., and Blundell, T. L. (1993) Comparative protein modelling by satisfaction of spatial restraints. *J Mol Biol* **234**, 779-815
5. Schneidman-Duhovny, D., Hammel, M., and Sali, A. (2010) FoXS: a web server for rapid computation and fitting of SAXS profiles. *Nucleic Acids Res* **38**, W540-544
6. Schneidman-Duhovny, D., Hammel, M., Tainer, J. A., and Sali, A. (2013) Accurate SAXS profile computation and its assessment by contrast variation experiments. *Biophys J* **105**, 962-974
7. Erzberger, J. P., Stengel, F., Pellarin, R., Zhang, S., Schaefer, T., Aylett, C. H., Cimermancic, P., Boehringer, D., Sali, A., Aebersold, R., and Ban, N. (2014) Molecular architecture of the 40SeIF1eIF3 translation initiation complex. *Cell* **158**, 1123-1135
8. Alber, F., Dokudovskaya, S., Veenhoff, L. M., Zhang, W., Kipper, J., Devos, D., Suprapto, A., Karni-Schmidt, O., Williams, R., Chait, B. T., Rout, M. P., and Sali, A. (2007) Determining the architectures of macromolecular assemblies. *Nature* **450**, 683-694
9. Shen, M. Y., and Sali, A. (2006) Statistical potential for assessment and prediction of protein structures. *Protein science : a publication of the Protein Society* **15**, 2507-2524
10. Shi, Y., Fernandez-Martinez, J., Tjioe, E., Pellarin, R., Kim, S. J., Williams, R., Schneidman-Duhovny, D., Sali, A., Rout, M. P., and Chait, B. T. (2014) Structural characterization by cross-linking reveals the detailed architecture of a coatomer-related heptameric module from the nuclear pore complex. *Molecular & cellular proteomics : MCP* **13**, 2927-2943
11. Fernandez-Martinez, J., Phillips, J., Sekedat, M. D., Diaz-Avalos, R., Velazquez-Muriel, J., Franke, J. D., Williams, R., Stokes, D. L., Chait, B. T., Sali, A., and Rout, M. P. (2012) Structure-function mapping of a heptameric module in the nuclear pore complex. *J Cell Biol* **196**, 419-434
12. Feng, S., Chen, J. K., Yu, H., Simon, J. A., and Schreiber, S. L. (1994) Two binding orientations for peptides to the Src SH3 domain: development of a general model for SH3-ligand interactions. *Science* **266**, 1241-1247
13. Kim*, S. J., Fernandez-Martinez*, J., Sampathkumar*, P., Martel, A., Matsui, T., Tsuruta, H., Weiss, T., Shi, Y., Markina-Inarrairaegui, A., Bonanno, J. B., Sauder, J. M., Burley, S. K., Chait, B. T., Almo, S. C., Rout, M. P., and Sali, A. (2014) Integrative structure-function mapping of the nucleoporin Nup133 suggests a conserved mechanism for membrane anchoring of the nuclear pore complex. *Molecular & cellular proteomics : MCP* **13**, 2911-2926
14. Rotkiewicz, P., and Skolnick, J. (2008) Fast procedure for reconstruction of full-atom protein models from reduced representations. *J Comput Chem* **29**, 1460-1465
15. Alber, F., Forster, F., Korkin, D., Topf, M., and Sali, A. (2008) Integrating diverse data for structure determination of macromolecular assemblies. *Annual review of biochemistry* **77**, 443-477

16. Webb, B., Lasker, K., Schneidman-Duhovny, D., Tjioe, E., Phillips, J., Kim, S. J., Velazquez-Muriel, J., Russel, D., and Sali, A. (2011) Modeling of proteins and their assemblies with the integrative modeling platform. *Methods in molecular biology* **781**, 377-397
17. Russel, D., Lasker, K., Webb, B., Velazquez-Muriel, J., Tjioe, E., Schneidman-Duhovny, D., Peterson, B., and Sali, A. (2012) Putting the pieces together: integrative modeling platform software for structure determination of macromolecular assemblies. *PLoS biology* **10**, e1001244
18. Ward, A. B., Sali, A., and Wilson, I. A. (2013) Biochemistry. Integrative structural biology. *Science* **339**, 913-915
19. Molnar, K. S., Bonomi, M., Pellarin, R., Clinthorne, G. D., Gonzalez, G., Goldberg, S. D., Goulian, M., Sali, A., and DeGrado, W. F. (2014) Cys-scanning disulfide crosslinking and bayesian modeling probe the transmembrane signaling mechanism of the histidine kinase, PhoQ. *Structure* **22**, 1239-1251
20. Schneidman-Duhovny, D., Pellarin, R., and Sali, A. (2014) Uncertainty in integrative structural modeling. *Current opinion in structural biology* **28**, 96-104
21. Kosinski, J., von Appen, A., Ori, A., Karius, K., Muller, C. W., and Beck, M. (2015) Xlink Analyzer: software for analysis and visualization of cross-linking data in the context of three-dimensional structures. *Journal of structural biology* **189**, 177-183
22. Fischer, H., Neto, M. D., Napolitano, H. B., Polikarpov, I., and Craievich, A. F. (2010) Determination of the molecular weight of proteins in solution from a single small-angle X-ray scattering measurement on a relative scale. *Journal of Applied Crystallography* **43**, 101-109

Figure S1

A

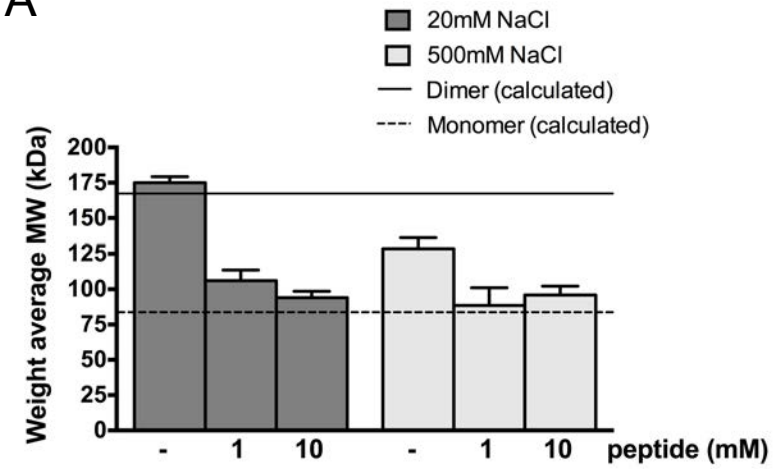
20mM NaCl
500mM NaCl
Dimer (calculated)
Monomer (calculated)
Weight average MW (kDa)
200
175
150
125
100
75
50
25
0
-
1
10
-
1
10
peptide (mM)

B

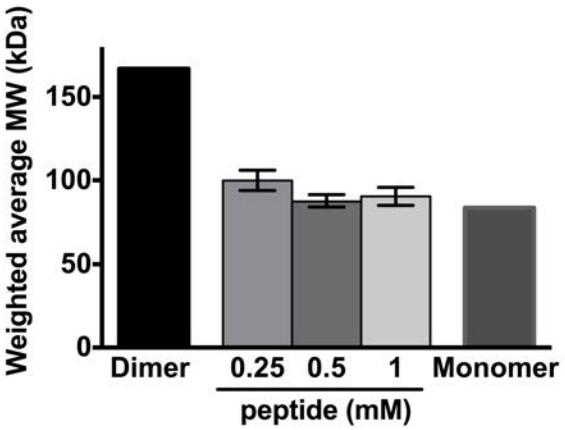
Weighted average MW (kDa)
150
100
50
0
Dimer
0.25
0.5
1
Monomer
peptide (mM)

Figure S2

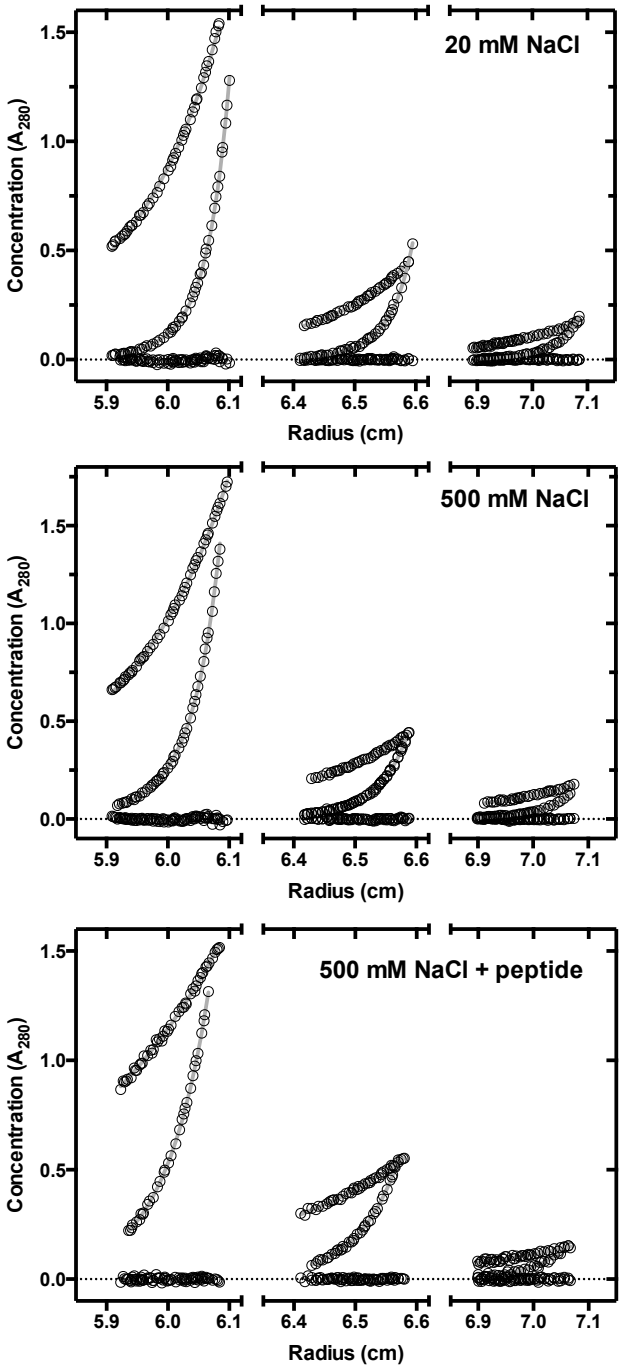
20 mM NaCl
500 mM NaCl
500 mM NaCl + peptide
Concentration (A_{280})
Radius (cm)
1.5
1.0
0.5
0.0
5.9
6.0
6.1
6.4
6.5
6.6
6.9
7.0
7.1

Figure S3

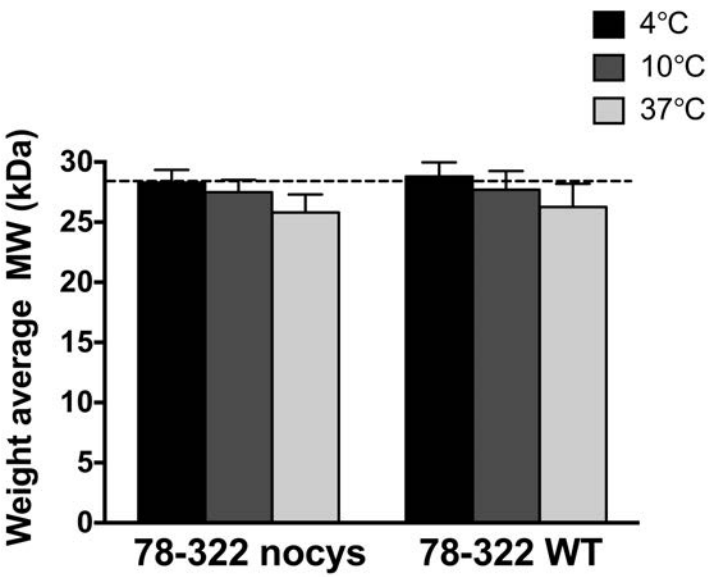
4°C
10°C
37°C
Weight average MW (kDa)
30
25
20
15
10
5
0
78-322 nocys
78-322 WT

Figure S4

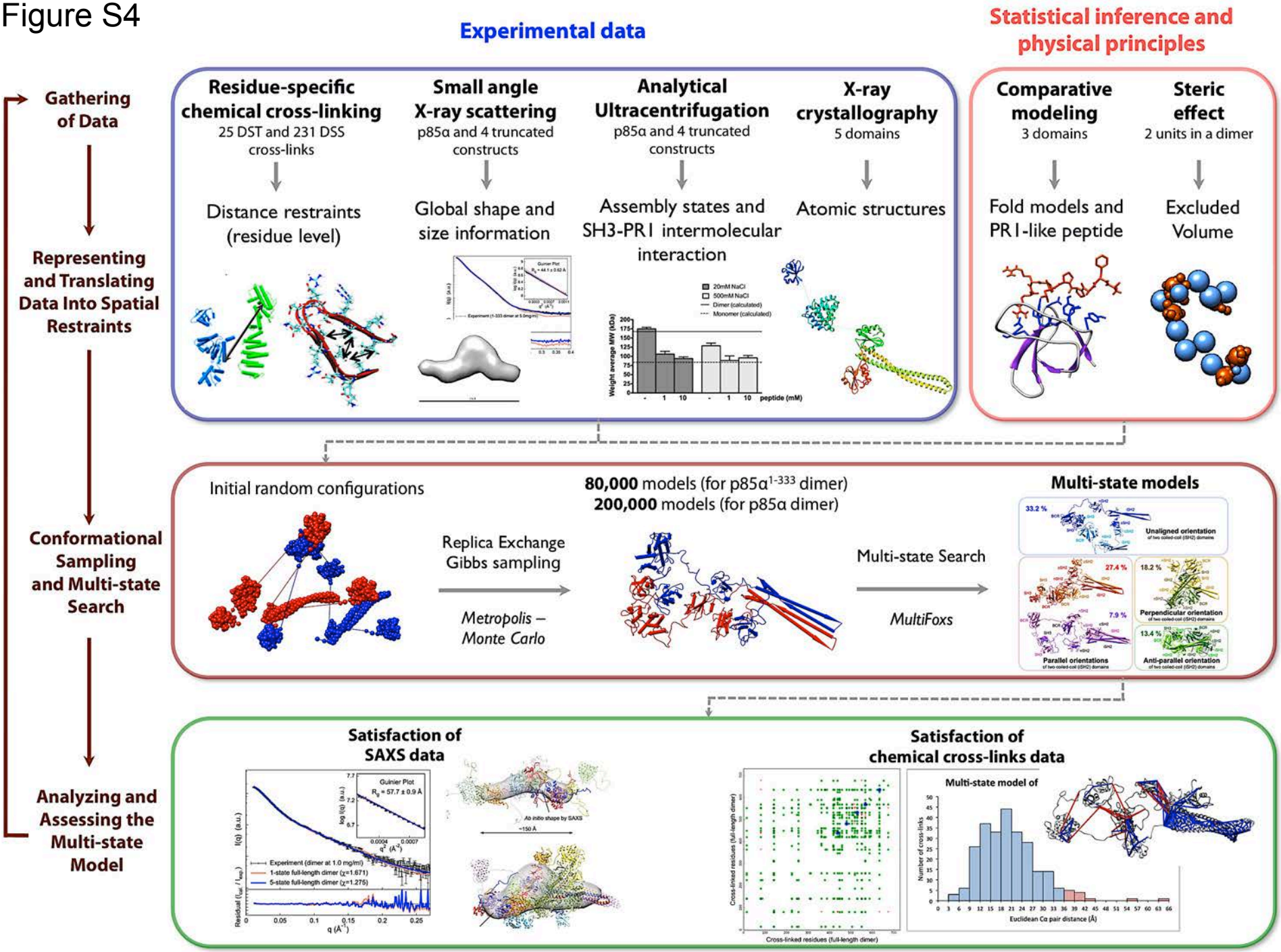
Experimental data
Statistical inference and physical principles
Gathering of Data
Representing and Translating Data Into Spatial Restraints
Conformational Sampling and Multi-state Search
Analyzing and Assessing the Multi-state Model
Residue-specific chemical cross-linking
25 DST and 231 DSS cross-links
Distance restraints (residue level)
Small angle X-ray scattering
p85α and 4 truncated constructs
Global shape and size information
Analytical Ultracentrifugation
p85α and 4 truncated constructs
Assembly states and SH3-PR1 intermolecular interaction
X-ray crystallography
5 domains
Atomic structures
Comparative modeling
3 domains
Fold models and PR1-like peptide
Steric effect
2 units in a dimer
Excluded Volume
Initial random configurations
Replica Exchange Gibbs sampling
Metropolis – Monte Carlo
80,000 models (for p85α1-333 dimer)
200,000 models (for p85α dimer)
Multi-state Search
MultiFoxs
Multi-state models
Unaligned orientation
Perpendicular orientation
Parallel orientations
Anti-parallel orientation
Satisfaction of SAXS data
Satisfaction of chemical cross-links data
Multi-state model of

Figure S5

Multi-state model of 1-333 dimer

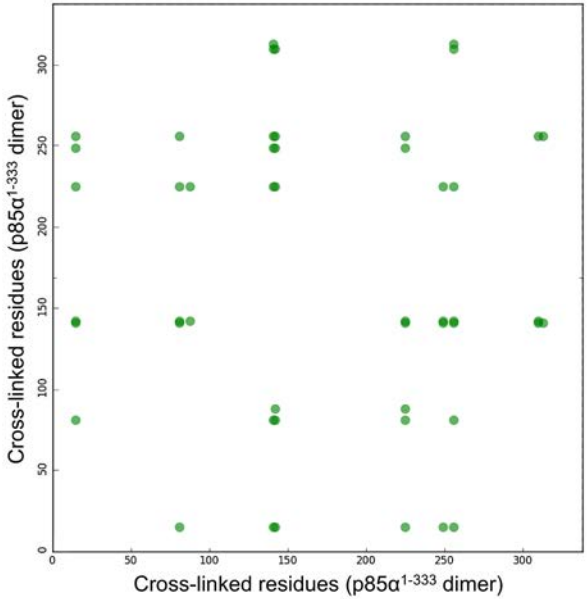

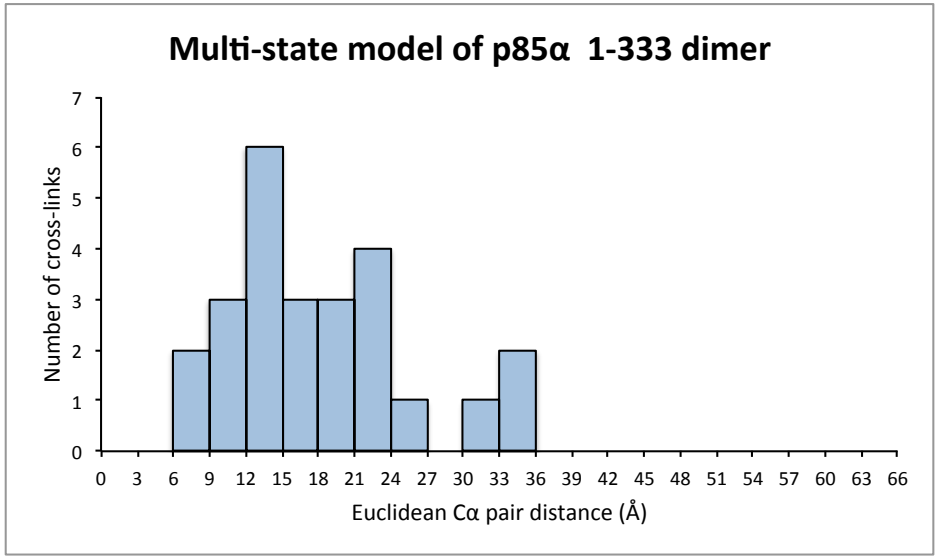

Multi-state model of Full-length dimer

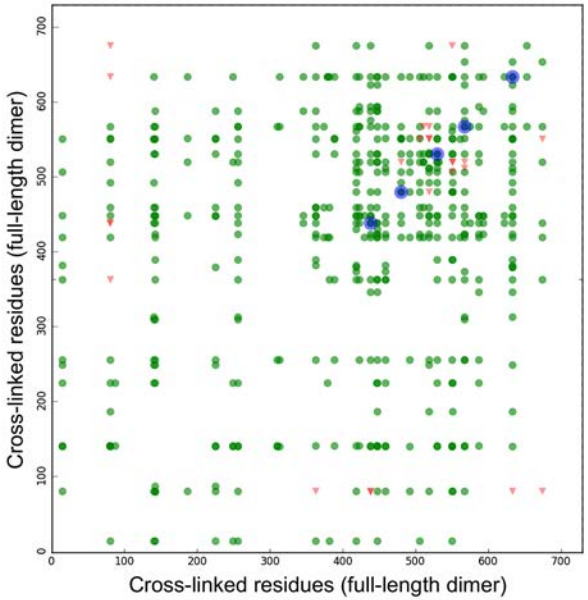

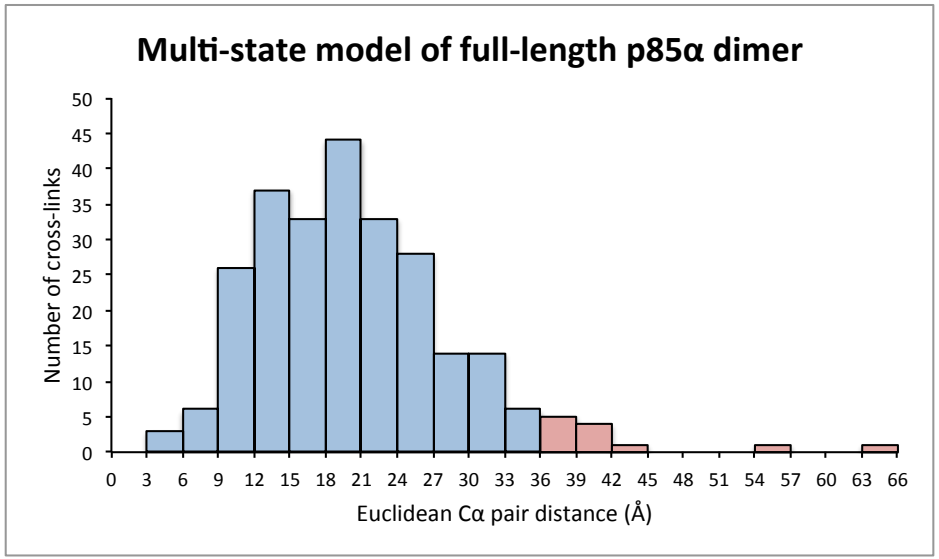

Figure S6

Conformational states
with cross-links satisfied (blue lines) or violated (red lines)

Population | **Combined** | **Assessment of the cross-links** | **Individual subunits**

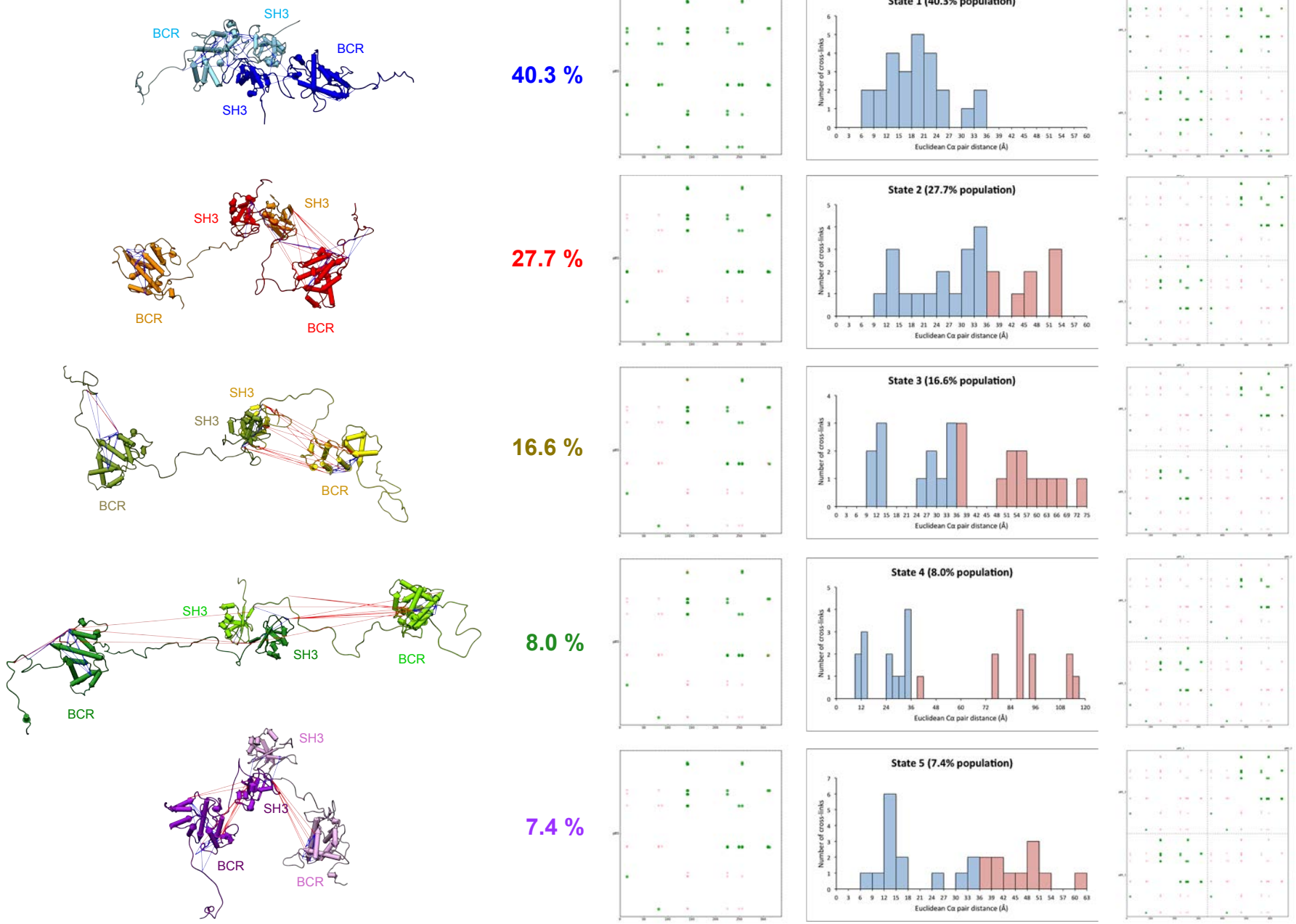

Figure S7

Conformational states
with cross-links satisfied (blue lines) or violated (red lines)

Population

Combined

Assessment of the cross-links

Individual subunits

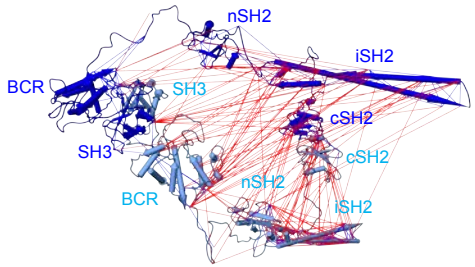

33.2 %

Unaligned orientatior
of two coiled-coil (iSH2) domain

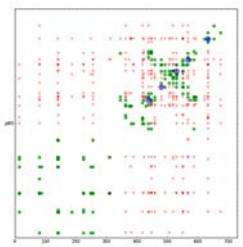

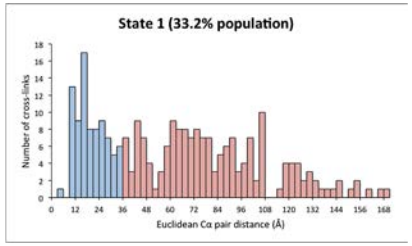

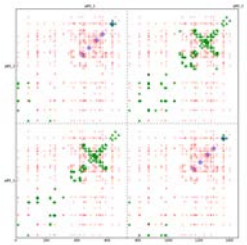

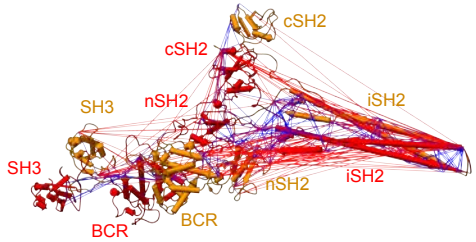

27.4 %

Parallel orientation
of two coiled-coil (iSH2) domains

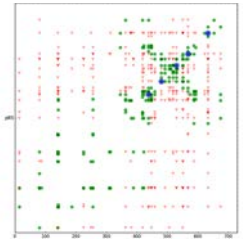

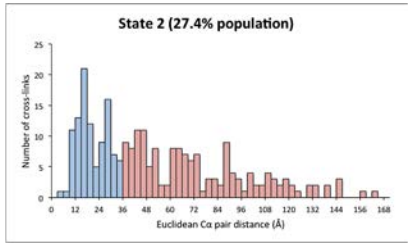

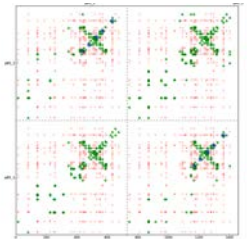

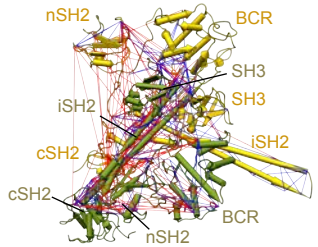

18.2 %

Perpendicular orientation
of two coiled-coil (iSH2) domains

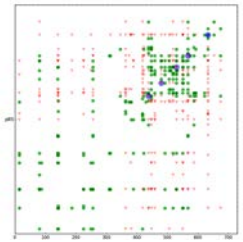

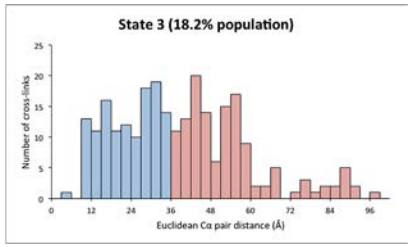

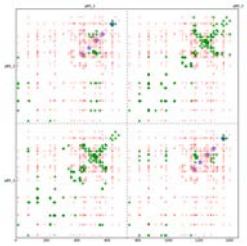

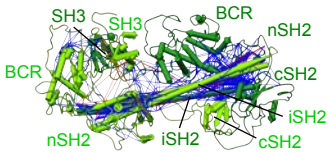

13.4 %

Anti-parallel orientation
of two coiled-coil (iSH2) domains

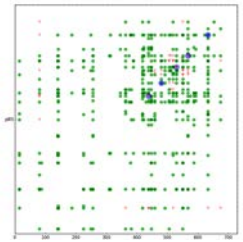

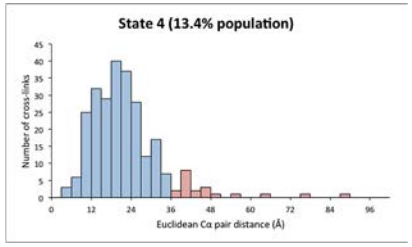

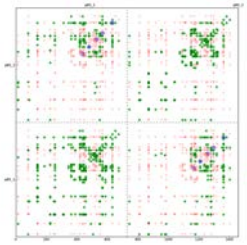

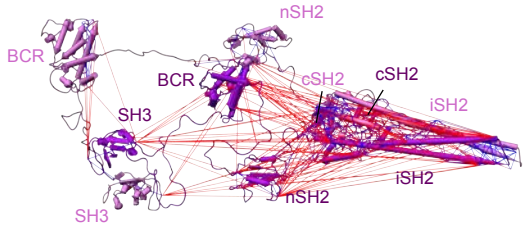

7.9 %

Parallel orientation
of two coiled-coil (iSH2) domains

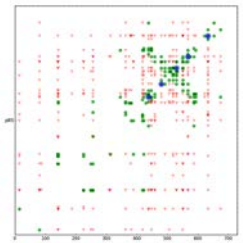

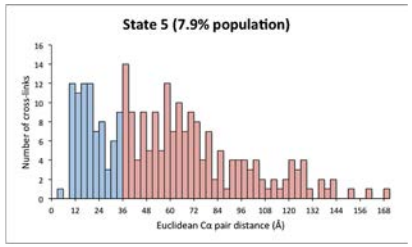

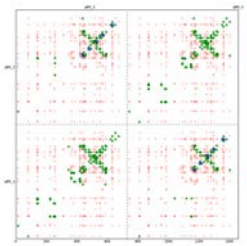

Table S1. Summary of SAXS analysis for the full-length p85α

Table A

Construct	NaCl	Concentration (mg/mL)	Concentration (μM)	10 °C *M.W.* (kDa)*	10 °C *Dmax* (Å)	10 °C *Rg* (Å)	25 °C *M.W.* (kDa)*	25 °C *Dmax* (Å)	25 °C *Rg* (Å)	*M.W.* from sequence monomer	*M.W.* from sequence dimer
1-724 full-length	**20 mM**	0.5 †	6.0 †	141.0	171.6	51.3	131.2	189.8	56.6	84 kDa	168 kDa
		1.0	12.0	**176.8**	199.1	59.5	153.8	193.6	57.7		
		1.5	18.0	199.0	206.6	62.7	**176.7**	199.8	60.4		
		2.0	24.0	207.1	209.7	63.0	191.0	210.1	63.2		
		5.0	60.0	289.1	232.7	70.7	303.9	238.0	72.3		

Table B

Construct	NaCl	Concentration (mg/mL)	Concentration (μM)	25 °C *M.W.* (kDa)*	25 °C *Dmax* (Å)	25 °C *Rg* (Å)	*M.W.* from sequence monomer	*M.W.* from sequence dimer
1-724 full-length	**500 mM**	0.5 †	6.0 †	96.4	174.7	54.0	84 kDa	168 kDa
		1.0	12.0	107.4	192.2	58.9		
		1.5	18.0	121.9	207.0	63.2		
		2.0	24.0	120.3	202.8	63.2		
		5.0	60.0	139.0	221.1	66.9		

Table C

Construct	NaCl	Concentration (mg/mL)	Concentration (μM)	10 °C + SH3-binding peptide *M.W.* (kDa)*	10 °C + SH3-binding peptide *Dmax* (Å)	10 °C + SH3-binding peptide *Rg* (Å)	25 °C + SH3-binding peptide *M.W.* (kDa)*	25 °C + SH3-binding peptide *Dmax* (Å)	25 °C + SH3-binding peptide *Rg* (Å)	*M.W.* from sequence monomer	*M.W.* from sequence dimer
1-724 full-length	**500 mM**	0.5 †	6.0 †	85.9	196.8	60.9	70.9	173.1	54.3	84 kDa	168 kDa
		1.0	12.0	**84.1**	178.7	55.8	80.0	175.9	54.6		
		1.5	18.0	92.3	191.8	57.1	**83.9**	190.1	55.8		
		2.0	24.0	90.3	183.7	55.9	88.1	184.1	55.4		
		5.0	60.0	104.9	195.2	58.2	97.6	196.9	58.3		

The SAXS parameters obtained under the conditions favoring the dimer state were highlighted in brown, while those obtained under the monomer condition in blue.
* Molecular Weights (*M.W.*) were estimated using SAXS MOW with a threshold of Qmax = 0.2~0.3 (1/Å), depending on the data.
† SAXS data has a higher noise at low concentrations (~0.5 mg/mL) than at high concentrations.
Radius of gyrations (*Rg*) were calculated in real space using DATGNOM in the ATSAS package.

Table S2. Summary of SAXS analysis for p85α$^{1\text{-}333}$ and p85α$^{78\text{-}322}$

Table A

Construct	NaCl	Concentration (mg/mL)	Concentration (μM)	10 °C *M.W.* (kDa)*	10 °C *Dmax* (Å)	10 °C *Rg* (Å)	10 °C + SH3-binding peptide *M.W.* (kDa)*	10 °C + SH3-binding peptide *Dmax* (Å)	10 °C + SH3-binding peptide *Rg* (Å)	*M.W.* from sequence monomer	*M.W.* from sequence dimer
1-333	**20 mM**	0.5 †	13.3 †	60.0	151.5	43.3	38.3	120.9	34.6	38 kDa	75 kDa
		0.75	19.9	67.5	150.8	43.1					
		1.0	26.5	69.2	154.3	44.1	**37.5**	121.1	34.9		
		2.0	53.0	72.4	157.1	44.9	40.8	124.5	34.9		
		3.5	92.8	77.5	161.2	46.3	45.5	123.8	35.4		
		5.0	132.5	**75.9**	155.1	44.3	46.4	122.4	35.0		

Table B

Construct	NaCl	Concentration (mg/mL)	Concentration (μM)	25 °C *M.W.* (kDa)*	25 °C *Dmax* (Å)	25 °C *Rg* (Å)	25 °C + SH3-binding peptide *M.W.* (kDa)*	25 °C + SH3-binding peptide *Dmax* (Å)	25 °C + SH3-binding peptide *Rg* (Å)	*M.W.* from sequence monomer	*M.W.* from sequence dimer
1-333	**500 mM**	0.5 †	13.3 †	64.4	158.1	43.7				38 kDa	75 kDa
		0.75	19.9	57.6	164.0	46.1	33.7	128.5	37.3		
		1.0	26.5				**36.1**	139.9	38.2		
		2.0	53.0	69.2	156.0	44.6	42.8	128.5	36.7		
		3.5	92.8	**75.9**	167.0	47.7	47.1	139.8	39.9		
		5.0	132.5	80.9	170.5	48.7	49.9	142.9	40.8		

Table C

Construct	NaCl	Concentration (mg/mL)	Concentration (μM)	10 °C *M.W.* (kDa)*	10 °C *Dmax* (Å)	10 °C *Rg* (Å)	*M.W.* from sequence monomer	*M.W.* from sequence dimer
78-322	**20 mM**	0.5 †	17.4 †	31.0	75.8	24.8	28 kDa	55 kDa
		1.0	34.7	**31.2**	88.8	26.3		
		1.5	52.1	31.7	83.7	25.8		
		2.0	69.4	33.3	129.8	28.1		
		5.0	173.5	34.2	100.3	28.1		

Table D

Construct	NaCl	Concentration (mg/mL)	Concentration (μM)	10 °C *M.W.* (kDa)*	10 °C *Dmax* (Å)	10 °C *Rg* (Å)	*M.W.* from sequence monomer	*M.W.* from sequence dimer
78-322	**500 mM**	0.5 †	17.4 †	31.7	83.3	26.6	28 kDa	55 kDa
		1.0	34.7	32.0	101.7	28.0		
		1.5	52.1	31.2	97.3	27.9		
		2.0	69.4	**30.8**	87.4	26.9		
		5.0	173.5	31.8	95.7	27.4		

The SAXS parameters obtained under the conditions favoring the dimer state were highlighted in brown, while those obtained under the monomer condition in blue.
* Molecular Weights (*M.W.*) were estimated using SAXS MOW with a threshold of Qmax = 0.2~0.3 (1/Å), depending on the data.
† SAXS data has a higher noise at low concentrations (~0.5 mg/mL) than at high concentrations.
Radius of gyrations (*Rg*) were calculated in real space using DATGNOM in the ATSAS package.

Table S3. Summary of SAXS analysis for p85α$^{1-432}$ and p85α$^{1-600}$

Table A

Construct	NaCl	Concentration (mg/mL)	Concentration (μM)	10 °C *M.W.* (kDa)*	10 °C *Dmax* (Å)	10 °C *Rg* (Å)	10 °C + SH3-binding peptide *M.W.* (kDa)*	10 °C + SH3-binding peptide *Dmax* (Å)	10 °C + SH3-binding peptide *Rg* (Å)	*M.W.* from sequence monomer	*M.W.* from sequence dimer
1-432	**20 mM**	0.5 †	10.3 †	68.2	137.7	42.7	51.0	135.0	39.6	49 kDa	98 kDa
		1.0	20.5	74.7	157.9	47.2	**51.1**	134.9	39.5		
		1.5	30.8	78.3	166.2	48.8	51.3	134.1	39.3		
		2.0	41.0	81.4	172.1	49.2	51.4	137.6	39.7		
		5.0	102.5	**93.9**	186.5	53.4	52.5	138.1	40.1		

Table B

Construct	NaCl	Concentration (mg/mL)	Concentration (μM)	10 °C *M.W.* (kDa)*	10 °C *Dmax* (Å)	10 °C *Rg* (Å)	10 °C + SH3-binding peptide *M.W.* (kDa)*	10 °C + SH3-binding peptide Dmax (Å)	10 °C + SH3-binding peptide Rg (Å)	*M.W.* from sequence monomer	*M.W.* from sequence dimer
1-432	**500 mM**	0.5 †	10.3 †	72.4	173.5	50.5	48.1	132.3	42.3	49 kDa	98 kDa
		1.0	20.5	66.7	166.3	51.1	**51.4**	153.0	45.7		
		1.5	30.8	72.3	181.1	54.0	53.5	158.8	46.0		
		2.0	41.0	77.0	181.7	54.4	53.0	157.1	46.7		
		5.0	102.5	84.7	188.7	56.4	51.8	160.5	45.9		

Table C

Construct	NaCl	Concentration (mg/mL)	Concentration (μM)	10 °C *M.W.* (kDa)*	10 °C *Dmax* (Å)	10 °C *Rg* (Å)	10 °C + SH3-binding peptide *M.W.* (kDa)*	10 °C + SH3-binding peptide *Dmax* (Å)	10 °C + SH3-binding peptide *Rg* (Å)	*M.W.* from sequence monomer	*M.W.* from sequence dimer
1-600	**20 mM**	0.5 †	7.2 †	97.3	159.4	48.8	69.3	138.4	44.5	70 kDa	140 kDa
		1.0	14.3	109.1	178.0	54.0	79.8	167.0	48.6		
		1.5	21.5	126.1	195.1	58.1	82.9	176.7	50.0		
		2.0	28.6	**130.5**	203.1	59.2	85.2	181.2	51.2		
		5.0	71.5	175.8	234.9	69.1	93.9	188.1	54.1		

Table D

Construct	NaCl	Concentration (mg/mL)	Concentration (μM)	10 °C *M.W.* (kDa)*	10 °C *Dmax* (Å)	10 °C *Rg* (Å)	10 °C + SH3-binding peptide *M.W.* (kDa)*	10 °C + SH3-binding peptide *Dmax* (Å)	10 °C + SH3-binding peptide *Rg* (Å)	*M.W.* from sequence monomer	*M.W.* from sequence dimer
1-600	**500 mM**	0.5 †	7.2 †	90.4	188.3	57.7	83.3	199.2	56.3	70 kDa	140 kDa
		1.0	14.3	113.9	213.2	63.6	81.2	181.8	53.8		
		1.5	21.5	117.2	223.0	65.6	84.5	191.7	56.2		
		2.0	28.6	121.2	221.7	65.6	82.5	187.9	55.9		
		5.0	71.5	**135.8**	236.5	70.5	83.8	197.3	57.5		

The SAXS parameters obtained under the conditions favoring the dimer state were highlighted in brown, while those obtained under the monomer condition in blue.

* Molecular Weights (*M.W.*) were estimated using SAXS MOW with a threshold of Qmax = 0.2~0.3 (1/Å), depending on the data.

† SAXS data has a higher noise at low concentrations (~0.5 mg/mL) than at high concentrations.

Radius of gyrations (*Rg*) were calculated in real space using DATGNOM in the ATSAS package.

Table S4. Restraint subsets for the p85α$^{1-333}$ dimer

Subset index	Sampling index	DST 1-333 XLs	Single SH3-PR1	Double SH3-PR1	Number of runs	Models generated per each run	Models generated in total
1	1-2		Y		2	9,800	19,600
2	3-4	Y	Y		2	9,800	19,600
3	5-6			Y	2	9,800	19,600
4	7-8	Y		Y	2	9,800	19,600
				Sum	8		78,400

Table S5. Restraint subsets for the full-length p85α dimer

Subset index	Sampling index	DST 1-333 XLs	DSS 1-724 XLs	Parallel iSH2 XLs	Anti-parallel iSH2 XLs	Homodimer cSH2 XL	Starting Model	Double SH3-PR1	Number of runs	Models generated per each run	Models generated in total
1	1 - 3			Y		Y	Random	Y	3	10,000	30,000
2	4 - 6	Y		Y		Y	Random	Y	3	1,000	3,000
3	7 - 9		Y	Y		Y	Random	Y	3	500	1,500
4	11 - 13				Y	Y	Random	Y	3	10,000	30,000
5	14 - 16	Y			Y	Y	Random	Y	3	1,000	3,000
6	17 - 19		Y		Y	Y	Random	Y	3	500	1,500
7	21 - 23					Y	Random	Y	3	10,000	30,000
8	24 - 26	Y				Y	Random	Y	3	1,000	3,000
9	27 - 29		Y			Y	Random	Y	3	500	1,500
10	31 - 33			Y		Y	1-333, 40.3%	Y	3	10,000	30,000
11	37 - 39		Y	Y		Y	1-333, 40.3%	Y	3	500	1,500
12	41 - 43				Y	Y	1-333, 40.3%	Y	3	10,000	30,000
13	47 - 49		Y		Y	Y	1-333, 40.3%	Y	3	500	1,500
14	51 - 53					Y	1-333, 40.3%	Y	3	10,000	30,000
15	57 - 59		Y			Y	1-333, 40.3%	Y	3	500	1,500
								Sum	45		198,000

Table S6. Representation of the p85α domains for integrative multi-state modeling

5 Domains		Representations	11 Segments	
			5 structured segments	6 disordered segments
			begins at ends at	begins at ends at
SH3	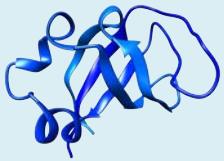	1-1: flexible string of a bead (DISOPRED) 2-82: Rigid Body, PDB, 3I5R_A (100% seq identity) PDB, 1PRL_C (30% seq identity)	2 - 82	1 - 1
PR1 motif		83-116: flexible string of beads (DISOPRED)		83 - 116
BCR	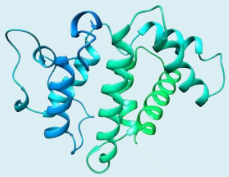	117-298: Rigid Body, PDB, 1PBW_A (100% seq id)	117 - 298	
PR2 motif		299-323: flexible string of beads (DISOPRED)		299 - 323
nSH2	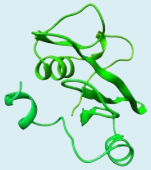	324-427: Rigid Body, PDB, 2IUG_A (100% seq id) PDB, 3HIZ_B (100% seq id) PDB, 3HHM_B (100% seq id)	324 - 427	
Linker		428-438: flexible string of beads (DISOPRED)		428 - 438
iSH2	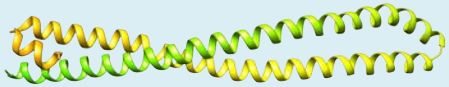	439-599: Rigid Body, PDB, 2V1Y_B (100% seq id) PDB, 3HIZ_B (100% seq id) PDB, 3HHM_B (100% seq id) PDB, 2Y3A_B (73% seq id)	439 - 599	
Linker		600-615: flexible string of beads (DISOPRED)		600 - 615
cSH2	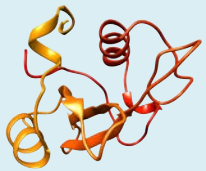	616-720: Rigid Body, PDB, 1H9O_A (100% seq id) PDB, 2Y3A_B (73% seq id) 721-724: flexible string of beads (DISOPRED)	616 - 720	721 - 724

Table S7. Consistency between the 25 DST chemical cross-links and the multi-state model of the p85α$^{1-333}$ dimer

	25 DST cross-linked pairs			Minimum Cα pair distance [Å] for each state				
	Residue 1	Residue 2	Shortest Pair Distance [Å] in the Multi-state Model	State 1	State 2	State 3	State 4	State 5
p85α 1-333 dimer	15	81	**11.1**	26.8	28.4	11.1	11.5	15.8
	15	225	**21.6**	21.6	43.9	59.3	77.7	41.8
	81	225	**20.9**	20.9	51.6	73.0	94.1	38.8
	88	225	**19.3**	19.3	53.1	48.5	77.1	44.8
	141	15	**21.9**	21.9	31.2	52.8	89.6	50.3
	141	81	**21.3**	21.3	35.1	56.8	112.0	36.1
	141	225	**32.9**	32.9	32.9	32.9	32.9	32.9
	142	15	**20.8**	20.8	33.1	51.4	88.7	53.8
	142	81	**17.5**	17.5	38.2	56.1	111.4	39.2
	142	88	**13.5**	13.5	51.1	38.9	89.3	47.1
	142	225	**34.8**	34.8	34.8	34.8	34.8	34.8
	249	15	**15.5**	15.5	37.8	62.3	89.7	48.5
	249	141	**11.6**	11.6	11.6	11.6	11.6	11.6
	249	142	**13.4**	13.4	13.4	13.4	13.4	13.4
	249	225	**24.3**	24.3	24.3	24.3	24.3	24.3
	256	15	**11.6**	11.6	45.4	63.3	94.0	60.3
	256	81	**22.2**	22.2	46.2	67.3	114.9	48.6
	256	141	**14.3**	14.3	14.3	14.3	14.3	14.3
	256	142	**13.2**	13.2	13.2	13.2	13.2	13.2
	256	225	**34.6**	34.6	34.6	34.6	34.6	34.6
	310	141	**13.1**	21.0	16.4	36.5	34.6	13.1
	310	142	**12.6**	19.7	18.5	36.8	35.6	12.6
	310	256	**7.0**	7.7	23.7	34.3	24.9	7.0
	313	141	**17.0**	17.8	24.1	28.5	40.9	17.0
	313	256	**6.8**	6.8	30.1	29.4	29.3	14.2

Table S8. Consistency between the combined 256 (25 DST and 231 DSS) chemical cross-links and the multi-state model of the full-length p85α dimer

	Combined 256 (25 DST and 231 DSS) cross-linked pairs			Minimum Cα pair distance [Å] for each state				
	Residue 1	Residue 2	Shortest Pair Distance [Å] in the Multi-state Model	State 1	State 2	State 3	State 4	State 5
Full-length p85α dimer	15	81	**18.8**	26.8	26.6	26.8	26.8	18.8
	15	225	**21.6**	21.6	52.0	21.6	21.6	38.9
	81	225	**20.9**	20.9	37.3	20.9	20.9	40.4
	81	551	**26.0**	120.5	145.2	31.5	26.0	139.9
	88	225	**19.3**	19.3	41.8	19.3	19.3	37.9
	141	15	**21.9**	21.9	32.9	21.9	21.9	71.3
	141	81	**12.9**	21.3	12.9	21.3	21.3	69.3
	141	225	**27.3**	32.9	27.3	32.9	32.9	32.9
	141	550	**24.6**	106.5	89.4	43.8	24.6	100.9
	142	15	**20.8**	20.8	35.3	20.8	20.8	73.4
	142	80	**16.8**	17.5	16.8	17.5	17.5	68.4
	142	81	**13.1**	17.5	13.1	17.5	17.5	71.7
	142	88	**13.5**	13.5	17.7	13.5	13.5	68.7
	142	225	**24.9**	34.8	24.9	34.8	34.8	34.8
	142	550	**26.5**	105.6	89.5	40.7	26.5	104.3
	187	81	**22.4**	22.4	28.0	22.4	22.4	56.4
	187	448	**27.2**	74.2	67.6	52.0	27.2	70.2
	187	519	**28.2**	144.1	145.2	46.4	28.2	152.0
	187	551	**29.5**	105.2	103.1	50.4	29.5	107.3
	187	633	**34.5**	104.7	72.6	81.0	34.5	74.6
	249	15	**15.5**	15.5	36.0	15.5	15.5	62.9
	249	141	**11.6**	11.6	11.6	11.6	11.6	11.6
	249	142	**13.4**	13.4	13.4	13.4	13.4	13.4
	249	225	**24.3**	24.3	24.3	24.3	24.3	24.3
	249	519	**30.8**	155.3	132.5	39.3	30.8	136.0
	249	633	**22.0**	102.6	63.2	91.8	22.0	61.0
	256	15	**11.6**	11.6	37.0	11.6	11.6	73.2
	256	81	**22.2**	22.2	23.4	22.2	22.2	67.7
	256	141	**14.3**	14.3	14.3	14.3	14.3	14.3
	256	142	**13.2**	13.2	13.2	13.2	13.2	13.2
	256	225	**20.4**	34.6	20.4	34.6	34.6	34.6
	256	423	**20.0**	58.2	22.3	22.1	20.0	20.5
	256	519	**24.4**	154.5	124.3	34.8	24.4	141.4
	256	530	**11.1**	142.7	111.2	31.6	11.1	127.2
	256	550	**21.3**	117.8	83.0	33.6	21.3	101.2
	256	567	**22.4**	96.2	60.6	51.3	22.4	84.7
	310	141	**12.3**	34.1	23.9	21.8	12.3	45.2
	310	142	**10.3**	33.4	24.8	22.4	10.3	44.6
	310	256	**11.6**	25.1	16.4	11.6	13.3	40.5
	310	567	**15.0**	99.5	48.0	32.4	15.0	57.5
	313	141	**14.8**	46.3	31.7	29.4	14.8	37.4
	313	256	**18.8**	37.2	21.6	19.8	18.8	33.1
	313	567	**9.1**	101.6	61.6	29.8	9.1	71.0
	313	633	**21.1**	106.3	55.0	67.0	21.1	79.4
	346	633	**29.1**	79.3	29.1	77.7	33.8	50.0
	363	15	**25.5**	49.8	66.5	45.3	25.5	46.1
	363	81	**41.2**	41.9	63.3	41.2	50.3	65.8
	363	142	**24.9**	37.9	43.6	40.4	24.9	52.7
	363	256	**26.8**	42.9	40.1	43.5	26.8	41.2
	363	382	**12.0**	12.0	12.0	12.0	12.0	12.0
	363	419	**27.9**	27.9	27.9	27.9	27.9	27.9
	363	423	**27.1**	27.1	27.1	27.1	27.1	27.1
	363	448	**18.5**	46.9	50.9	43.7	18.5	59.7
	363	459	**20.5**	62.6	63.9	49.3	20.5	74.9
	363	530	**25.4**	120.0	115.8	58.6	25.4	125.8
	363	550	**32.2**	90.7	88.8	52.9	32.2	102.3
	363	567	**16.7**	66.5	64.9	43.4	16.7	77.3
	363	587	**19.0**	36.5	39.8	36.8	19.0	46.8
	363	633	**17.4**	79.4	40.5	82.9	17.4	70.1
	379	225	**31.4**	62.1	43.3	41.1	31.4	44.0
	379	633	**20.9**	67.7	38.4	88.9	20.9	59.0
	382	15	**16.4**	52.2	73.2	36.5	16.4	52.4
	389	142	**13.6**	44.4	33.6	27.9	13.6	39.1
	389	256	**20.6**	44.1	30.0	32.9	20.6	29.4
	389	363	**16.1**	16.1	16.1	16.1	16.1	16.1
	389	530	**25.8**	128.2	108.3	54.1	25.8	127.5
	389	550	**24.3**	99.2	80.7	56.7	24.3	98.4
	389	551	**24.5**	97.0	80.5	56.3	24.5	97.5
	389	633	**23.2**	73.4	53.2	85.3	23.2	78.6
	419	15	**16.0**	58.8	86.0	28.7	16.0	64.7
	419	81	**32.8**	48.7	74.6	52.2	32.8	86.6
	419	142	**14.5**	56.3	27.9	39.5	14.5	33.4
	419	374	**9.8**	9.8	9.8	9.8	9.8	9.8
	419	379	**11.5**	11.5	11.5	11.5	11.5	11.5
	419	382	**16.0**	16.0	16.0	16.0	16.0	16.0
	419	448	**12.5**	50.5	27.9	56.9	12.5	45.7
	419	480	**21.8**	92.1	61.8	63.5	21.8	84.4
	419	506	**11.7**	123.7	93.4	54.8	11.7	116.4
	419	511	**16.3**	131.1	102.0	57.2	16.3	125.1
	419	519	**13.1**	134.2	105.3	56.0	13.1	126.7
	419	530	**10.5**	119.8	89.7	56.0	10.5	111.4
	419	550	**19.9**	91.1	62.0	55.0	19.9	83.1
	419	561	**12.8**	76.0	47.9	59.9	12.8	67.9
	419	567	**7.1**	69.4	37.9	64.1	7.1	58.0
	419	633	**17.0**	57.6	48.9	96.9	17.0	65.3
	423	142	**12.3**	63.3	19.0	31.9	12.3	32.0
	423	506	**19.6**	124.7	101.4	44.7	19.6	112.5
	423	519	**18.3**	129.8	112.4	45.0	18.3	122.1
	423	567	**13.4**	65.9	42.9	56.0	13.4	52.9
	423	633	**27.9**	67.1	47.3	86.6	27.9	63.8
	430	419	**17.8**	26.2	17.8	32.3	22.8	25.1
	430	448	**21.9**	34.9	34.5	29.6	21.9	24.9
	438	80	**41.6**	63.3	93.8	56.9	41.6	95.0
	438	81	**40.7**	64.7	90.6	55.1	40.7	92.3
	438	141	**27.0**	70.8	45.5	53.1	27.0	46.5
	438	142	**26.2**	71.6	48.0	55.6	26.2	50.3
	438	256	**20.3**	76.4	45.0	51.0	20.3	49.0
	438	346	**17.6**	17.6	26.2	32.2	22.0	26.2
	438	363	**22.6**	28.7	33.6	43.5	22.6	48.4
	438	419	**16.6**	39.2	20.4	45.9	16.6	41.4
	438	423	**17.3**	32.1	17.3	34.5	21.8	33.7
	438	438	**18.5**	124.7	19.8	89.4	87.7	18.5
	438	448	**10.0**	19.0	18.3	20.4	10.0	15.8
	438	459	**23.8**	33.6	32.5	36.0	23.8	30.7
	438	480	**34.9**	64.2	62.7	37.1	34.9	58.1
	438	519	**16.2**	107.2	105.7	40.8	16.2	95.2
	438	530	**10.0**	91.2	89.3	30.9	10.0	80.4
	438	567	**29.0**	38.3	36.2	39.7	29.0	36.7
	438	575	**18.6**	26.9	24.2	27.8	18.6	25.6
	438	587	**6.9**	10.9	6.9	11.0	8.5	9.2
	438	633	**14.2**	72.9	43.2	35.7	14.2	40.3
	447	142	**20.2**	79.8	54.1	44.8	20.2	62.5
	447	225	**32.3**	86.5	69.5	57.2	32.3	54.1
	447	363	**21.6**	44.9	48.5	46.5	21.6	58.2
	447	419	**12.4**	49.2	27.3	58.1	12.4	45.3
	447	423	**20.0**	43.7	27.3	47.5	20.0	38.7
	447	438	**7.7**	16.7	15.6	18.8	7.7	13.0
	447	459	**18.2**	18.2	18.2	18.2	18.2	18.2
	447	519	**18.0**	91.2	91.0	26.0	18.0	79.1
	447	530	**4.2**	75.4	74.8	14.4	4.2	64.4
	447	633	**9.8**	76.9	49.9	42.6	9.8	42.2
	448	15	**30.5**	95.6	115.1	51.6	30.5	95.6
	448	81	**31.2**	80.8	104.9	39.4	31.2	103.3
	448	141	**17.8**	78.5	52.2	46.6	17.8	61.6
	448	142	**17.6**	78.5	53.6	44.6	17.6	65.3
	448	225	**33.0**	86.4	69.9	54.0	33.0	55.1
	448	256	**11.8**	91.0	48.9	42.5	11.8	65.7
	448	346	**23.4**	28.8	42.1	42.2	23.4	37.6

	Combined 256 (25 DST and 231 DSS) cross-linked pairs			Minimum Cα pair distance [Å] for each state				
	Residue 1	Residue 2	Shortest Pair Distance [Å] in the Multi-state Model	State 1	State 2	State 3	State 4	State 5
Full-length p85α dimer	448	423	**18.2**	45.6	28.2	46.7	18.2	38.8
	448	480	**26.2**	47.2	47.2	26.2	26.7	41.2
	448	506	**22.7**	82.2	81.0	31.5	22.7	73.8
	448	519	**19.7**	88.9	88.4	27.5	19.7	77.1
	448	530	**6.3**	73.2	72.2	14.0	6.3	62.2
	448	550	**27.4**	43.9	43.9	29.3	27.4	35.5
	448	567	**21.0**	21.0	21.0	21.0	21.0	21.0
	448	633	**12.6**	76.0	51.5	41.7	12.6	45.6
	459	81	**30.2**	95.4	120.5	36.3	30.2	118.8
	459	141	**21.4**	87.9	67.0	47.0	21.4	75.6
	459	142	**23.3**	87.7	68.0	45.8	23.3	79.2
	459	225	**25.3**	99.9	84.9	45.9	25.3	69.9
	459	256	**16.8**	100.4	62.2	48.0	16.8	78.4
	459	363	**20.5**	62.6	63.9	49.3	20.5	74.9
	459	374	**12.5**	56.6	41.0	62.8	12.5	51.8
	459	382	**18.8**	62.9	51.9	55.0	18.8	66.4
	459	419	**11.2**	66.2	36.1	67.0	11.2	57.7
	459	423	**12.8**	61.0	40.7	57.8	12.8	52.5
	459	506	**28.2**	67.3	65.3	28.2	34.8	61.6
	459	511	**31.9**	75.6	73.9	31.9	41.5	68.9
	459	519	**27.9**	73.7	73.7	27.9	35.8	63.7
	459	551	**13.9**	26.9	26.9	26.9	13.9	20.4
	459	567	**9.5**	9.5	9.5	9.5	9.5	9.5
	459	633	**8.7**	75.6	67.4	48.3	8.7	49.5
	480	480	**14.7**	160.6	14.7	50.9	28.0	18.9
	480	506	**34.7**	38.5	34.7	38.5	38.5	38.5
	480	519	**42.2**	44.6	44.2	44.6	44.6	42.2
	480	550	**9.9**	9.9	9.9	9.9	9.9	9.9
	480	551	**11.4**	11.4	11.4	11.4	11.4	11.4
	480	633	**22.3**	83.9	96.8	48.9	22.3	69.6
	492	81	**18.6**	137.5	164.0	18.6	32.3	161.1
	492	141	**25.0**	117.4	108.4	34.3	25.0	122.4
	492	256	**11.5**	128.2	100.4	31.5	11.5	123.1
	492	419	**20.5**	107.3	76.3	60.0	20.5	98.1
	492	480	**18.3**	18.3	18.3	18.3	18.3	18.3
	492	506	**17.4**	21.2	17.4	21.2	21.2	21.2
	492	519	**29.7**	30.3	29.7	30.3	30.3	30.3
	492	530	**16.6**	16.6	16.6	16.6	16.6	16.6
	492	551	**21.7**	25.0	25.0	25.0	25.1	21.7
	492	633	**13.1**	90.5	113.8	58.6	13.1	78.0
	506	15	**31.2**	170.8	194.9	37.5	31.2	168.1
	506	550	**36.5**	39.3	38.5	37.6	39.3	36.5
	506	551	**34.2**	42.2	41.3	34.2	42.2	37.2
	506	633	**21.0**	107.0	130.4	72.5	21.0	96.2
	511	519	**13.0**	13.0	13.0	13.0	13.0	13.0
	511	633	**26.6**	114.7	138.5	76.9	26.6	104.1
	519	81	**34.2**	165.0	190.0	34.2	39.9	182.2
	519	506	**15.8**	15.8	15.8	15.8	15.8	15.8
	519	511	**13.0**	13.0	13.0	13.0	13.0	13.0
	519	530	**16.8**	16.8	16.8	16.8	16.8	16.8
	519	550	**38.4**	45.1	45.1	45.1	45.1	38.4
	519	551	**38.4**	47.0	47.0	42.5	47.0	38.4
	519	633	**22.5**	119.9	133.3	68.0	22.5	107.8
	530	141	**21.3**	132.1	118.0	33.3	21.3	128.2
	530	142	**20.0**	130.9	117.8	31.3	20.0	131.4
	530	225	**31.8**	151.1	139.1	57.8	31.8	120.4
	530	480	**26.5**	28.1	28.1	28.1	28.1	26.5
	530	506	**16.4**	17.7	16.4	17.7	17.7	17.7
	530	511	**21.8**	22.7	21.8	22.7	22.7	22.7
	530	519	**16.8**	16.8	16.8	16.8	16.8	16.8
	530	530	**12.7**	196.1	12.7	68.3	76.3	18.6
	530	550	**21.7**	29.5	29.2	29.5	29.5	21.7
	530	551	**22.1**	31.3	31.3	31.3	31.3	22.1
	530	633	**7.6**	106.8	118.6	55.6	7.6	93.6
	532	519	**19.9**	19.9	19.9	19.9	19.9	19.9
	550	15	**31.2**	138.6	158.5	36.2	31.2	135.1
	550	81	**24.9**	121.3	146.3	29.2	24.9	141.4
	550	141	**24.6**	106.5	89.4	43.8	24.6	100.9
	550	225	**19.0**	123.0	110.0	41.5	19.0	92.5
	550	551	**3.8**	3.8	3.8	3.8	3.8	3.8
	550	561	**10.3**	16.1	16.1	16.1	10.6	10.3
	550	633	**22.6**	88.2	92.5	53.5	22.6	72.6
	551	225	**17.3**	122.7	109.2	44.4	17.3	90.4
	551	480	**11.4**	11.4	11.4	11.4	11.4	11.4
	567	81	**26.0**	96.1	121.7	27.0	26.0	120.0
	567	141	**20.6**	84.2	67.2	42.3	20.6	82.1
	567	142	**23.7**	83.6	67.7	44.5	23.7	85.7
	567	256	**22.4**	96.2	60.6	51.3	22.4	84.7
	567	374	**15.1**	60.3	44.5	58.3	15.1	53.5
	567	423	**13.4**	65.9	42.9	56.0	13.4	52.9
	567	480	**20.6**	28.4	27.3	26.7	20.6	21.6
	567	506	**33.7**	61.9	60.8	33.7	40.4	58.0
	567	511	**38.7**	70.5	69.3	38.7	46.7	65.8
	567	519	**36.4**	69.9	69.9	36.4	40.2	62.0
	567	530	**24.3**	54.4	53.4	24.3	25.9	45.7
	567	551	**14.8**	24.6	24.6	24.6	14.8	16.3
	567	567	**18.8**	146.7	18.8	54.0	38.1	18.8
	567	633	**13.4**	72.6	71.3	46.2	13.4	54.0
	575	567	**12.8**	12.8	12.8	12.8	12.8	12.8
	587	142	**28.2**	65.8	47.0	44.9	28.2	56.9
	587	225	**21.9**	72.9	57.2	55.6	21.9	51.1
	587	256	**26.5**	78.4	40.7	53.3	26.5	55.2
	587	346	**14.5**	24.9	29.9	32.3	14.5	25.7
	587	419	**16.0**	42.7	16.0	43.8	20.9	30.5
	587	423	**13.5**	37.9	13.5	32.9	23.0	24.6
	587	447	**13.6**	15.1	15.1	15.1	15.1	13.6
	587	448	**15.2**	15.2	15.2	15.2	15.2	15.2
	587	519	**18.3**	100.6	100.4	40.7	18.3	90.9
	587	530	**17.8**	84.9	83.9	28.6	17.8	75.4
	587	567	**30.7**	30.7	30.7	30.7	30.7	30.7
	587	633	**23.6**	66.7	47.1	29.0	23.6	41.0
	593	423	**19.9**	38.9	19.9	43.6	20.3	34.5
	593	438	**5.5**	11.5	11.3	16.0	5.5	14.6
	593	447	**11.2**	11.2	11.2	11.2	11.2	11.2
	593	448	**13.4**	13.4	13.4	13.4	13.4	13.4
	593	587	**11.9**	11.9	11.9	11.9	11.9	11.9
	593	633	**15.3**	68.4	51.3	36.5	15.3	36.9
	622	438	**11.8**	60.7	36.7	21.8	11.8	35.1
	622	448	**19.0**	63.9	47.0	26.3	19.0	35.1
	622	567	**10.9**	57.9	65.9	34.6	10.9	41.0
	622	633	**16.3**	16.3	16.3	16.3	16.3	16.3
	633	81	**54.6**	101.6	93.9	76.7	54.6	122.1
	633	141	**26.4**	95.2	58.4	87.2	26.4	58.5
	633	379	**20.9**	67.7	38.4	88.9	20.9	59.0
	633	382	**18.7**	69.8	42.7	87.4	18.7	67.2
	633	550	**22.6**	88.2	92.5	53.5	22.6	72.6
	633	551	**21.7**	89.4	89.4	51.3	21.7	69.9
	633	633	**17.4**	18.4	17.4	18.7	20.0	19.7
	653	567	**22.2**	70.8	71.5	40.4	22.2	47.3
	653	633	**16.1**	16.1	16.1	16.1	16.1	16.1
	674	81	**63.2**	84.7	79.7	67.3	63.2	109.6
	674	363	**14.7**	62.5	19.3	82.3	14.7	63.8
	674	419	**26.1**	46.4	32.2	91.5	26.1	57.4
	674	438	**20.4**	57.1	31.2	30.7	20.4	21.5
	674	519	**18.1**	106.8	131.3	51.6	18.1	88.8
	674	550	**40.8**	74.0	87.5	52.7	40.8	57.5
	674	567	**24.8**	59.9	64.5	33.8	24.8	38.5
	674	653	**11.6**	11.6	11.6	11.6	11.6	11.6